J of Nuclear Medicine Technology, first published online March 15, 2021 as doi:10.2967/jnmt.120.261862

PET/MR Part 2: Technological Principles

Currie G[1,2], Kamvosoulis P[3] & Bushong, S[2]

[1]School of Dentistry and Health Science, Charles Sturt University, Wagga Wagga, Australia

[2]Department of Radiology, Baylor College of Medicine, Houston, USA

[3]Magnetic Resonance Department, New York-Presbyterian / Weill Cornell Medical Center, New York, USA

Keywords: PET/MR, PET, MRI, PET/MRI

Footline: Principles of PET/MR

Learning objectives:

- demonstrate an understanding of the principles associated with PET/MRI instrumentation
- demonstrate an understanding of the advances and challenges associated with PET/MRI
- demonstrate strong conceptual understanding of the technologies driving PET/MRI from the context of implementation

Abstract

The challenges of hybridizing positron emission tomography (PET) and magnetic resonance imaging (MRI) as a simultaneous modality have been largely overcome in recent times. PET hybridized with magnetic resonance (MR) has seen the emergence of PET/MR imaging systems in the clinical setting and with it comes a responsibility to adapt appropriate facility design, safety practices, protocols and procedures, and clinical opportunity. This manuscript provides an insight into the considerations and challenges associated with PET/MR technology. Given the nature of PET is well established amongst the readership of this journal, the manuscript provides an introduction to the foundations of MRI instrumentation and emphasis on specific technological aspects of PET/MR systems. This manuscript is the second in a four-part integrated series sponsored by the SNMMI-TS PET/MR Task Force in conjunction with the SNMMI-TS Publication Committee; building on the previous article on establishing a facility (part 1). In subsequent editions, PET/MRI will be explored based on protocols and procedures (part 3), and applications and clinical cases (part 4).

Introduction

While the merits of single photon emission computed tomography (SPECT), positron emission tomography (PET), computed tomography (CT) and magnetic resonance imaging (MRI) have been widely recognized and reported in both research and clinical practice, the synergistic hybridization of imaging modalities has revolutionized diagnostic imaging. SPECT/CT and PET/CT are in widespread practice, merging the advantages of the high resolution anatomical information of the CT with the physiological and molecular level functional information from the nuclear medicine modalities. More recently, PET/MR hybrid imaging systems have emerged although PET/MR was devised and patented in the 1990s (*1*). The first integrated PET/MR imaging systems emerged in 2010 and by 2015 there were about 110 PET/MR imaging systems globally (160 approximately in 2020) with Siemens representing nearly 80% of the market ahead of Philips and GE (*2*). For clarification and consistency, the terms PET/MR and PET/MRI are not used interchangeably in this article. PET/MR is used in reference to the technology and principles while PET/MRI refers to the application of that technology in imaging. The use of MRI versus MR throughout should be self-explanatory. Furthermore, the term imaging system is used in preference to the more archaic use of the term scanner.

A working knowledge of PET is assumed in this discussion but can be refreshed in the previously published work of Turkington (*3*). The general principles of MRI are outlined below. This is also not a forum for debating the relative merits of PET/MRI against PET/CT. Nonetheless, it would be remiss not to highlight the motivations for PET/MRI, including (*1,4-7*):

1. PET/MRI produces a reduced patient radiation dose. This is particularly important in pediatric patients, women of child-bearing age, and the numerous patients who have sequential scanning to monitor response to therapy or recurrence. Compared to PET/CT, PET/MRI can reduce the dose to just 25% given that 75% of the patient radiation dose is associated with CT. An example would be the reduction in a pediatric whole body PET/CT scan from 19.5 mSv to 4.6 mSv for PET/MRI.
2. Soft tissue visualization and contrast is superior on MRI over CT, enhancing lesion detection and diagnostic accuracy in numerous conditions. MRI adds important

complementary functional information to the PET scan, further enhancing outcomes. The opportunity from PET/MRI for multiparametric imaging increases radiomic feature extraction and diagnostic utility.

3. PET/MR offers genuinely simultaneous imaging which has a positive impact on co-registration; especially moving organs (eg. heart and lungs), moving lesions due to physiological motion (eg. lung tumor), changing organs (eg. filling bladder) or after patient motion (eg. pain, anxiety). The simultaneous imaging also allows better synchronization of respiratory and cardiac gating between PET and MRI data, and the application of motion correction to the PET data. The correction for motion increases lesion detection and quantitative accuracy.
4. There is also a reported efficiency when PET and MRI are required since each is acquired simultaneous. In the absence of PET/MRI, PET/CT is sequential in nature and then would require the additional time of the stand alone MRI.
5. Image reconstruction offers the chance to correct partial volume artifacts on the PET images using the MRI co-registration. The net impact of this approach is resolution recovery or enhanced spatial resolution of the PET data.

Despite these advantages, replacing PET/CT with PET/MR is associated with a number of challenges including, without being limited to; detector function in a magnetic field, attenuation correction, scatter correction, artifacts and truncation of the field of view. This is especially true when considering truly integrated PET/MR with simultaneous acquisition (*1,4,5,7*).

Foundations of MRI

For the MRI novice, the basic foundations allow working knowledge of the principles of MRI. For some, the superficial introduction outlined below will provide sufficient insight. Others will yearn for deeper understanding beyond the scope and word limit of this article. Such insight can be sourced from a number of key textbooks (*8,9*). Rather than exploring Newtonian and quantum physics, a simpler model of MRI is offered.

MR Signal

Some nuclei spin on their own axis which allows them to be thought of as small magnets. Hydrogen is one such nuclei, indeed the one that produces the strongest "magnet". Consider the distribution of hydrogen in the human body. It is clear that hydrogen imaging would be both biologically useful for some tissues and sufficiently abundant distribution to allow quality imaging. The dispersion of hydrogen in objects is random and fairly uniform which means the small magnets in opposite alignments cancel one another out to produce a net zero magnetic vector (figure 1A). If a magnetic field (B_0) is applied to the object, then the hydrogen atoms align parallel with the magnetic field and the object has a net magnetic vector; it has become polarized (figure 1B) (*8-10*). In reality, not all hydrogen atoms (let's refer to them as proton dipoles) become aligned with the magnetic field. Approximately 1 per million of proton dipoles realign with the magnetic field but this is sufficient to create polarization (*8*). While a simple schematic representation like figure 1 suggests the atoms have aligned uniformly, in reality they wobble. The wobble is known as precession (figure 1C) and the frequency of the precession is called the Larmour frequency and depends on the strength of the magnetic field (*8-10*). For hydrogen, a 1.5 Tesla (T) MR imaging system produces 63.9 MHz precession while 3T produces 127.8 MHz precession (*8,9*). Indeed, this might be better expressed as a gyromagnetic ratio of MHz of precession per T. This is important because each dipole nucleus has a unique gyromagnetic ratio. For hydrogen (1H) it is 42.6 MHz/T while others include ^{19}F at 40.1 MHz/T, ^{31}P at 17.2 MHz/T, ^{23}Na at 11.3 MHz/T, and ^{13}C at 10.7 MHz/T.

Excitation

Consider the patient in an MR imaging system. In the presence of the magnetic field, proton dipoles align with the magnetic field to produce a net magnetic vector (figure 1B). This is also referred to as the equilibrium magnetization state. The magnetic field causes each dipole to randomly precess (figure 2A). If a pulse of radiofrequency (RF) is emitted at the Larmour frequency, it will change the energy state of the hydrogen nuclei (excitation) (*8-10*). This is achieved using the RF coil that pulses at resonance and causes the net magnetic vector to flip to negative on the Z axis. Despite this, the precession remains perpendicular to the Z axis but instead of being random, the precession of each dipole becomes in phase (figure 2B) (*8-10*). This is referred to as phase coherence and generates the optimal MR signal. The net magnetism returns to the equilibrium magnetism state (relaxation) (*8-10*). This creates a moving magnetic field, and electric current can then be generated in an RF receiver coil (figure 2C) (*8-10*). The time for the signal to return to equilibrium is called relaxation time and the signal produced is referred to as free induction decay (FID) (*8-10*).

Relaxation

Relaxation time is associated with two independent processes, T_1 and T_2, that occur simultaneously (*8-10*). T_1 relaxation is also known as longitudinal relaxation because it describes the rate at which the magnetism returns to equilibrium. T_2 relaxation is also known as transverse relaxation time because it describes the rate at which phase coherent precession de-phases. T_1 is the time required to return to 63% of equilibrium value after exposure to a 90^o RF pulse (*8-10*). Conversely, T_2 is the time required to de-phase the signal to 37% of its original value. The role of contrast media is to alter the relaxation times (figure 3) (*8-10*). Relaxivity measures the degree to which a given amount of contrast agent shortens T_1 or T_2 which means higher relaxivity produces better enhancement (*11*).

Image Formation

The FID signal intensity decreases over time as a harmonic oscillation (figure 4A) (*8*). Figure 4A represents signal intensity over time but this can be converted to the frequency domain via Fourier transformation to produce a nuclear magnetic resonance (NMR) spectrum (figure 4B). The clusters of signals at different frequencies represents the specific NMR characteristics of different tissues (figure 4C) (*8-10*). While this provides an insight into the proportion of various tissues in a sample (as used in NMR spectroscopy), it does not provide information about the location of those tissues. Superimposed on the static magnetic field (B_0), a gradient magnetic field (B_G) is applied with different field strengths and this allows tissue localization (figure 4D) (*8-10*). A far more complex FID is produced by data collected at multiple projections which can then be reconstructed using tomographic principles previously described (*12*).

Pulse Sequences

While this provides a simple explanation of the MRI process, in reality, FID is not a simple imaging option because of the weak signal (*8-10*). A one pulse sequence would need to be repeated several hundreds of times in order to generate an adequate signal (*8,9*). The time between each RF pulse is called the repetition time (TR) and if sufficient time elapses between each RF pulse, equilibrium allow the amplitude of successive FIDs to be equal (*8,9*). A short TR means equilibrium has not been reached and successive FIDs will have smaller amplitudes (partial saturation) (*8,9*).

Alternatively, multiple pulse sequences can be used. If the 90^o RF pulse is followed by a 180^o RF pulse, an echo signal of the FID can be generated by the re-phasing (*8,9*). The echo signal is termed spine echo (SE) and is stronger than the FID signal and it is measured at the peak time of echo (TE) (*8,9*). TE after the 180^o RF pulse is equal to the time between the 90^o RF pulse and the 180^o RF pulse (*8,9*). A multi-echo spin echo (MESE) pulse sequence could be used where a subsequent 180^o RF pulse followed the previous, producing another SE (*8,9*). An image can be generated from each of the SE (primary and secondary) at the respective TE to produce images of differing characteristics. The inversion recovery (IR) pulse sequence starts with a 180^o RF pulse

and follows it with a 90° RF pulse which inverts the net magnetism (*8,9*). There are a large variety of sequences used in MRI and the details are beyond the scope of this manuscript, however, those interested are encouraged to do further research on: gradient echo sequences, dual echo sequence, fluid attenuated inversion recovery (FLAIR) sequence, diffusion weighted sequences, short tau (TI) inversion recovery (STIR) sequence, and Dixon chemical shift.

PET/MR Technology

System design

One of the principal barriers to hybrid PET/MR imaging systems is the incompatibility of the technology. The traditional PET system design using photomultiplier tubes (PMTs) is susceptible to even small magnetic fields and, thus, incompatible with the large magnetic fields associated with MRI (*1,4-7*). Furthermore, the electronics associated with signal processing in PET can create interference in the MR signal (*4-7*). This limitation gives rise to a number of solutions or configurations. The first is to have separate PET and MRI systems linked by a single patient table with each gantry positioned and shielded sufficiently as to not interfere with the other (eg. Philips Ingenuity TF) (figure 5A). Alternatively, the detectors themselves could reside within the MRI system which are coupled by optical fibers to PMTs residing outside the magnetic field (figure 5B). This design may adopt a split magnet design allowing the optical fibers to be shorter and the magnet bore wider. The genuinely integrated option would modify detector composition to eliminate susceptibility from and to the magnetic field (eg. Siemens Biograph mMR, GE Healthcare SIGNA PET/MR and United Imaging uPMR 790 PET/MR). Clearly the integrated system is required to take advantage of simultaneous PET and MR imaging. One approach is to couple the scintillation detector directly or by optical fiber to avalanche photodiodes (APD) in RF shielding (figure 5C). Alternatively, silicon photomultiplier (SiPM) detectors can be coupled to the scintillation detector (figure 5D).

Commercial Systems

There are four commercially available clinical PET/MR imaging systems on the market. The GE Healthcare SIGNA™ PET/MR is an integrated system with 3T MR with PET (time of flight) that employs silicon photomultiplier (SiPM) detectors directly coupled to lutetium based crystals. The GE MR750w wide bore (70 cm) MRI system can be retro-fitted with a SiPM PET insert to produce a 6cm bore PET/MR device. The Siemens Biograph mMR PET/MR is an integrated system with 3T MR with PET that employs avalanche photo diodes (APD) detectors and lutetium oxyorthosilicate (LSO) crystals. The United Imaging uPMR 790 PET/MR is an integrated system with 3T MR with PET that employs SiPM detectors directly coupled to lutetium yttrium oxyorthosilicate (LYSO) crystals. The Phillips Ingenuity TF PET/MR is a sequential system with 3T MR co-located and sharing an imaging system bed with a LYSO and photomultiplier tube (PMT) based PET system.

Detectors

The traditional PET PMT was based on the coupling of bismuth germinate oxide (BGO) scintillation crystal detectors to PMTs. More recently the detectors have been upgraded to lutetium-based scintillators like LSO and LYSO. LSO and LYSO have faster scintillation decay which makes them more effective in high count rate conditions, in additional lines of response for 3D scanning, in longer axial fields of view, and for time of flight (*1,4,6,13*). LSO and LYSO have typically been coupled to PMTs. PMTs offer signal amplification but are susceptible to magnetic fields and are bulky; both significant issues for integrating PET into an MRI gantry. APDs are silicon semiconductors that are not only able to operate within the magnetic field but are also compact (*1,4,6,7,13*). Unfortunately APDs are thermally sensitive which requires thermal stabilization. Furthermore, the signal gain is very low compared to a traditional PMT which requires additional electronic signal amplification (*1,4,7,13*). Both these requirements have been successful in traditional sequential PET/CT imaging system design and with some difficulties for PET/MR design. For example, the additional electronics for signal boosting is MR sensitive, the thermal control creates bulk, and the low signal gain prohibits time of flight.

SiPMs are an alternative to the PMT and APDs although, technically, they are a type of APD (*1,7,13*). SiPMs are a silicon semiconductor detector operating in Geiger-mode (G-APD) and are also referred to in the literature as solid-state photomultipliers (SSPM) and multi pixel photon counters (MPPC) (figure 6A) (*1,7,13*). In the SiPM, the detector matrix is comprised of thousands of pixels that operate as a photon counter in Geiger-mode. The pixels are known as single-photon avalanche diodes (SPADs) and each individual SPAD can be counted independently and simultaneously with other SPADs (figure 6B) (*1,13*). This approach results in high resolution, high sensitivity, high signal gain, low noise, fast timing, less magnetic susceptibility, and time of flight capability (*1,13*).

Challenges of PET/MR

Even with the technical issues addressed, PET/MR comes with a number of challenges. Physical space, shielding and planning is a major challenge but has been detailed in the first article in this series (*14*) and will not be duplicated here. The time cost associated with imaging protocols and procedures will only briefly be discussed below since it will be detailed in part 3 of this series of articles.

Time Cost

Despite PET/MRI being considered simultaneous in nature, the MRI RF pulse sequences tend to be longer than PET bed positions (*1*). A three minute bed position, for example, may be insufficient time for all MRI sequences to be completed, although recent developments have seen emergence of 4-5 MRI sequences in a 3 min PET bed position. This discrepancy is exacerbated in whole body imaging typical of oncology studies. The solution under development is fast MRI protocols. These have shown some early success but have a number of barriers to overcome, including noise reduction. Nonetheless, multiple sequences for whole body MRI over 20 to 40 minutes have a higher time cost than the multi-bed position PET covering the same anatomy in 10-20 minutes (*1*). An important consideration in this discussion is the actual applications of PET/MRI which will be discussed in detail in part 4 of this series. Many of the clinical applications or clinical scenarios where PET/MRI provides a tangible benefit over PET/CT may only require a

single bed position. Neurological PET/MRI, cardiac PET/MRI or head and neck oncology imaging for example.

Attenuation Correction

A distinct advantage of PET/CT is the ability to perform accurate attenuation correction using a rapid CT acquisition immediately prior to or after the PET image. This was a significant advance over the previous methods using 68Ge/68Ga sources to produce transmissions scans prior to the patient being administered their PET radionuclide dose. PET/MRI has no option for producing a transmission scan for attenuation correction because there is no correlation between the attenuation coefficient and MR signal intensity (*1,5,6,15*). A variety of approaches have been adopted to create an MR based proxy for the attenuation map; each continues to be constrained by limitations. The challenge of accurate attenuation mapping using MRI is complicated by additional attenuation associated with MR hardware and coils in the field of view (*1,6*). Furthermore, attenuating structures on the PET image may be positioned outside the acquisition field; an arms down chest PET/MRI for example may truncate the MR signal from arms and, thus, be unable to estimate attenuation from the truncated tissues (*1,6*). The advantage of PET/MRI attenuation correction over PET/CT if it can be performed accurately is the reduced patient radiation dose and the simultaneous acquisition that can overcome mismatches between sequentially performed PET and CT attenuation map (*1*).

Simple segmentation and classification of different tissue types using the T_1 signal can be constrained by the lack of bone signal and associated attenuation correction (*1,5,7,15*). Moreover, some tissues like lung can have different attenuation coefficients from one person to the next (*1*). Another simple approach may be suitable for tissues with uniform attenuation (eg. the brain) using estimation methods and attenuation formula (*1*). This method was used for brains pre-PET/CT but the additional influence of MRI coils requires careful mapping of the coil template in the estimated attenuation corrections (*1,15*). It is possible to also revert to previous PET system designs where a rotating rod source (68Ge/68Ga) is used for a transmission scan (*1,15*). Obviously this approach adds

additional time associated with the transmission scan, noisy attenuation maps and remains inferior to CT based attenuation correction.

Current approaches for attenuation correction on integrated PET/MRI use a 3D Dixon approaches which provides in phase and out of phase data sets for water and fat (*6*). In essence, this allows segmentation of air, fat, muscle and lung tissue for attenuation coefficients but lacks accommodation of bone (*6*). Bone is classified as soft tissue from an attenuation coefficient perspective in this approach. The underestimation of attenuation associated with this bone non-classification can produce substantial errors in quantitation of both bone and adjacent soft tissue. This could be overcome with the addition of atlas-based methods but these have limitations around variations from "normal" anatomy not uncommon in pathological patients (*15*). A different approach incorporates ultra short echo signals to delineate bone and add to the standard T_1 tissue segmentation. The ultra short echo time approach can also be combined with Dixon sequence (MRI sequence based on chemical shift designed for fat suppression) to produce classes of very short T_2 tissues for segmentation (*5,6,15*). This approach has particular potential in lung imaging.

An important area of development for PET/MRI is in pseudo-CT attenuation maps (figure 7). There are a number of limitations in estimating an attenuation map from MRI for PET/MRI that convolutional neural networks (CNNs) may overcome (*16*). Deep CNNs can produce an attenuation map that closely models the CT based grounded truth (*17,18*). Others have integrated the Dixon method with a CNN to generate pseudo-CT for pelvic PET/MRI with promising results of less than 2% variation from the CT map (*19*). More accurate attenuation maps also resulted from the use of deep CNN combined with zero-echo-time Dixon pseudo-CT (*20*). CNN approaches can produce pseudo-CT attenuation maps from the PET sinogram and this approach was used successfully (less than 1% error) on 18F FDG brain scans (*21*).

The ability to accurately correct for attenuation is essential for accurate quantitation of PET data (*1,6*). Indeed, the accuracy of relative quantitation markers like standardized

uptake value (SUV) will be undermined if the integrity of attenuation correction is sacrificed.

Artifacts

Both PET and MRI are vulnerable to artifact and this can undermine not only image quality but quantitative accuracy. PET/MRI combined adds a layer of complexity to potential artifacts. The most common artifact that raises concern is cross-talk between PET and MRI but this has been largely overcome by the new detector designed discussed previously. It is possible mechanical misalignment can cause co-registration inaccuracies (*6*). Imperfect attenuation correction remains a concern for artifact production and this can be exacerbated by the administration of contrast by interfering with tissue segmentation (*6*). MRI is susceptible to signal voids associated with items like implants and these may also produce attenuation artifact on the PET scan (*6*). As already discussed, artifacts can be produced in the PET data by attenuation from the MRI hardware and coils, and by truncation of the field of view.

Conclusion

While hybrid imaging with PET/MR plays a role in a number of clinical situations, there are a number of technical considerations required in the design and operation of the imaging systems. Specifically, modifications to conventional imaging systems that accommodate integration of the two modalities without image degrading cross talk require deep understanding before adopting the technology. Such understanding will have translational benefits to procedural and clinical applications of PET/MRI. Specific design features of PET/MRI help guide facility planning detailed in part 1 of this series. The integration of PET/MRI affords the opportunity for enhanced protocols and clinical applications which will be explored in more detail in parts 3 and 4 of this series, respectively. Understanding the principles of PET, MRI and integrated PET/MR imaging systems provide the foundation for safe, effective and optimal adoption of PET/MR technology.

References

1. Vandenberghe S, Marsden PK. PET-MRI: a review challenges and solutions in the development of integrated multimodality imaging, *Physics in Medicine & Biology*. 2004; 60: R115-R154.
2. Fendler WP, CZernin J, Herrman K, Beyer T. Variations in PET/MRI operations results from an international survey among 39 active sites, *J Nucl Med*. 2016; 57: 2016-2021.
3. Turlington TG. Introduction to PET instrumentation, *J Nucl Med Technol*. 2001; 29: 1-8.
4. Wehrl HF, Sauter, AW, Judenhofer MS, Pichler BJ. Combined PET/MR imaging – technology and applications, *Technology in cancer research and treatment*, 2010; 9: 5-20.
5. Herzog H. PET/MRI: challenges, solutions and perspectives, *Z Med Phys*. 2012; 22: 281–298 http://dx.doi.org/10.1016/j.zemedi.2012.07.003
6. Quick HH. Integrated PET/MR, *J MRI*. 2014; 39: 243-258.
7. Disselhorst JA, Bezrukov I, Kolb A, Parl C, Pichler BJ. Principles of PET/MR imaging, *J Nucl Med*. 2014; 55: 2S-10S.
8. Bushong SC, Clarke G. Magnetic resonance imaging: physical principles and biological principles, 4th edn, 2015, Elsevier, St Louis.
9. Hashemi RH, Bradley WG, Lisanti CJ. MRI the basics, 2nd edn, 2004, Lippincott Williams & Wilkins, Philadelphia.
10. van Geuns RJM, Wielopolski PA, de Bruin HG et al. Basic principles of magnetic resonance imaging, *Progress in Cardiovascular Diseases*, 1999; 42: 149-156.
11. Currie G. Pharmacology part 5: CT and MRI contrast, *Journal of Nuclear Medicine Technology*. 2019; 47: 189-202.
12. Currie G, Hewis J, Bushong S. Tomographic reconstruction; a non-mathematical overview, *Journal of Medical Imaging and Radiation Sciences*, 2015; 46: 403-412.
13. Gundacker S, Heering A. The silicon photomultiplier: fundamentals and applications of a modern solide-state photon detector, *Physics in Medicine & Biology*. 2020; 65: 17TR01.
14. Kamvosoulis P, Currie G. PET/MR part 1: establishing a PET/MR facility, *Journal of Nuclear Medicine Technology*. 2021; 48: under review.
15. Martinez-Moller A, Nekolla SG. Attenuation correction for PET/MR: problems, novel approaches and practical solutions, *Z Med Phys*. 2012; 22: 299-310 http://dx.doi.org/10.1016/j.zemedi.2012.08.003
16. Currie G. Intelligent Imaging: artificial intelligence augmented nuclear medicine, *Journal of Nuclear Medicine Technology*. 2019; 47: 217-222.
17. Hwang et al. Improving the Accuracy of Simultaneously Reconstructed Activity and Attenuation Maps Using Deep Learning. *J Nucl Med.* 2018; 59: 1624–1629.

18. Hwang D, Kang SK, Kim KY, Seo S, Paeng JC, Lee DS, Lee JS. Generation of PET attenuation map for whole-body time-of-flight ^{18}F-FDG PET/MRI using a deep neural network trained with simultaneously reconstructed activity and attenuation maps. *J Nucl Med*. 2019 Jan 25. pii: jnumed.118.219493. doi: 10.2967/jnumed.118.219493. [Epub ahead of print]

19. Torrado-Carvajal A, Vera-Olmos J, Izquierdo-Garcia D, Catalano OA, Morales MA, Margolin J, Soricelli A, Salvatore M, Malpica N, Catana C. Dixon-VIBE Deep Learning (DIVIDE) Pseudo-CT Synthesis for Pelvis PET/MR Attenuation Correction. *J Nucl Med*. 2019: 60: 429-435.

20. Leynes A et al. Zero-Echo-Time and Dixon Deep Pseudo-CT (ZeDD CT): Direct Generation of Pseudo-CT Images for Pelvic PET/MRI Attenuation Correction Using Deep Convolutional Neural Networks with Multiparametric MRI. *J Nucl Med* 2018; 59: 852–858.

21. Liu F, Jang H, Kijowski R, Zhao G, Bradshaw T, McMillan AB. A deep learning approach for ^{18}F-FDG PET attenuation correction. *EJNMMI Phys*. 2018; 12: 24. doi: 10.1186/s40658-018-0225-8.

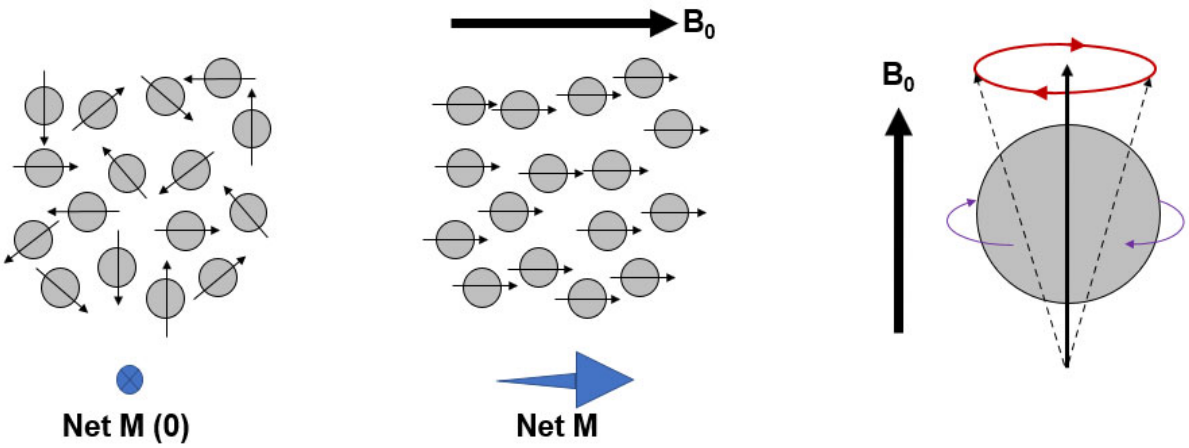

Figure 1: Nuclei spin creates polarity with random distribution producing a net magnetic vector (M) of zero (left). Application of a strong magnetic field (B_0) creates alignment of proton dipoles producing a net M aligned with B_0 (middle). While proton dipoles spin on their axis (purple arrows) to produce the small magnets, in the presence of a magnetic field the movement is gyromagnetic (red arrows) and termed precession (right).

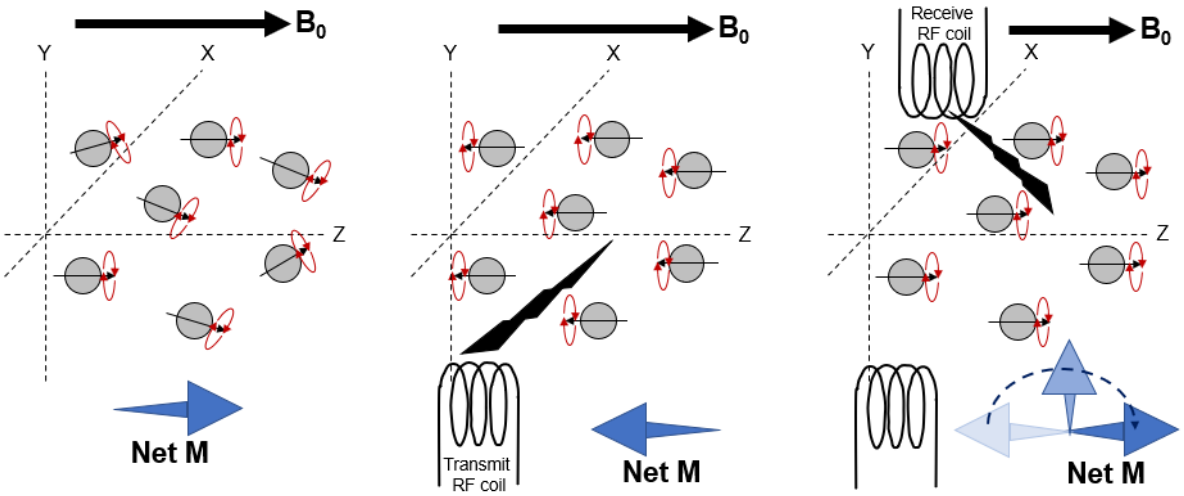

Figure 2: Nuclei spin creates polarity with a magnetic field (B_0) and positive alignment of proton dipoles with the Z axis producing a net magnetic vector (M) and random precession (left). The RF transmission causes the aligned proton dipoles to flip to negative on the Z axis and causes the precession to come into phase (middle). Relaxation results in reversion of the net M producing a free induction decay signal at the RF receiver coil (right).

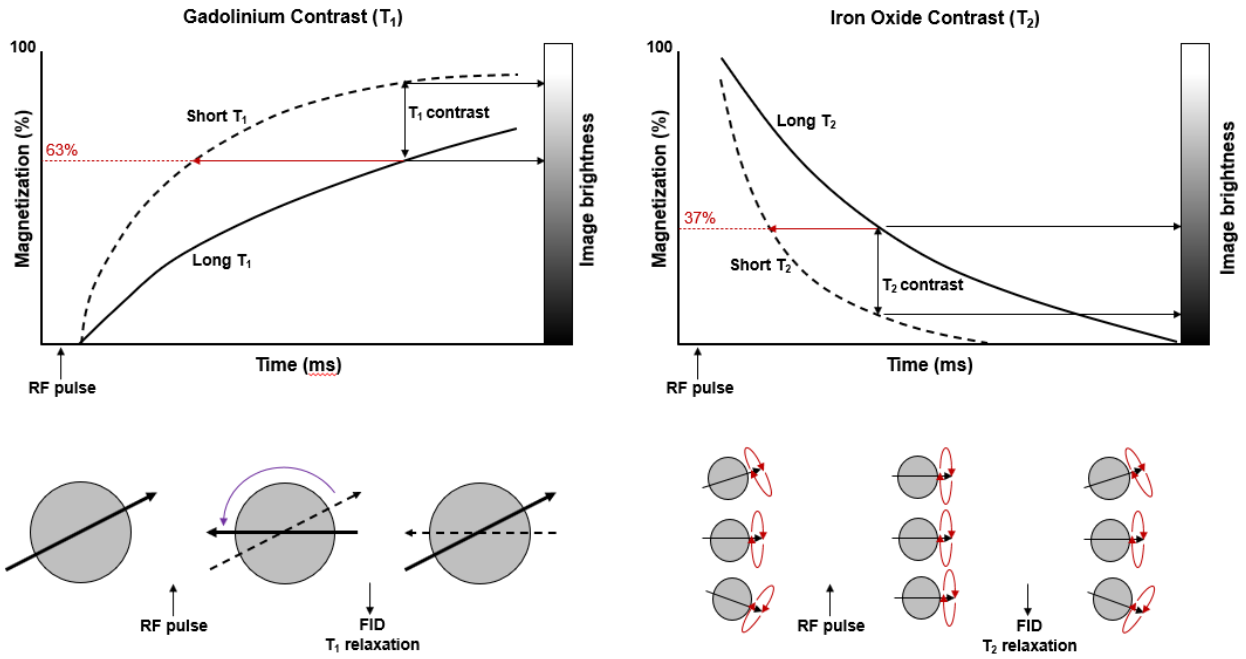

Figure 3: Schematic representation of the principle of T_1 and T_2 contrast enhancement by altering relaxation times. The T_1 plot (top left) shows the effect of shortening the relaxation time with gadolinium contrast and the resultant positive enhancement of the contrast. Likewise, the T_2 plot (top right) shows the effect of shortening the relaxation time with iron oxide contrast and the resultant negative enhancement of the contrast. Image adapted with permission (*11*).

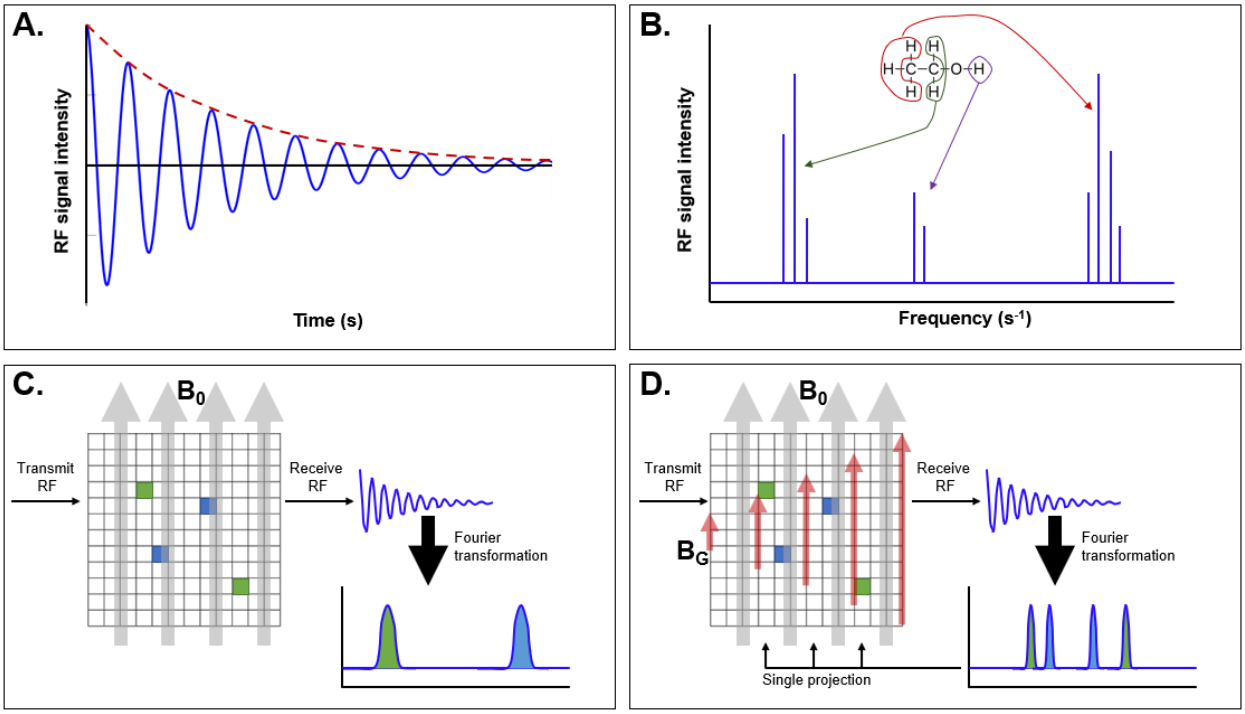

Figure 4: (A) The free induction decay (FID) with decreasing harmonic oscillation. (B) Fourier transformation of the FID creates a frequency domain NMR spectrum. For MRI, clusters representing different tissue which is schematically represented here for NMR spectroscopy where each cluster represents a different molecular array of hydrogen (as depicted with red, green and purple hydrogen atoms). (C) In a static magnetic field (B_0) the NMR spectrum identifies different tissues but not spatial location. (D) Application of a gradient magnetic field (B_G) depicted in red allows spatial identification for that gradient projection. Rotating the gradient magnetic field allows multiple projections to be collected and reconstructed.

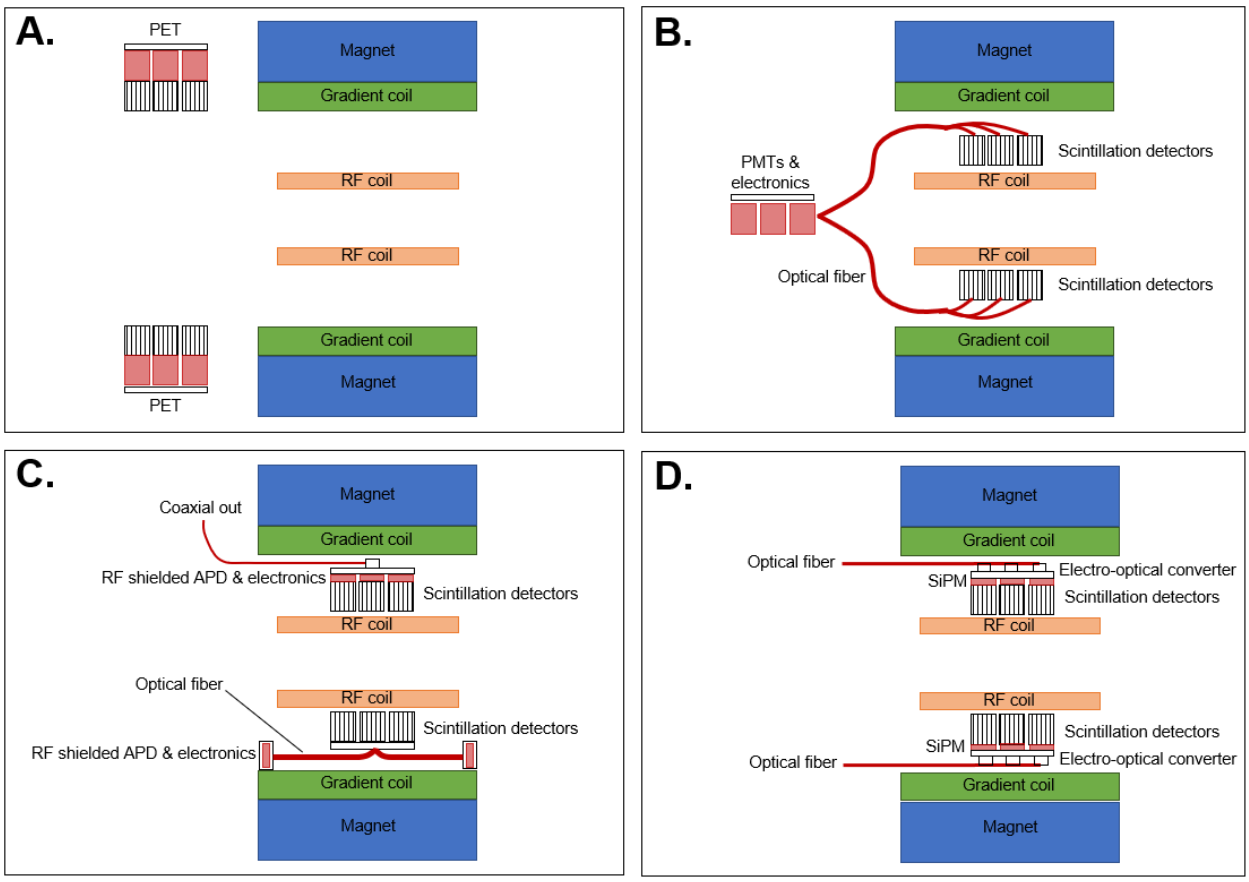

Figure 5: (A) Separate but linked PET/MR without the option for simultaneous acquisition. (B) Integrated and simultaneous PET/MR housing the RF sensitive PMTs and electronics outside of the gantry. (C) Two versions of the integrated PET/MR using RF shielded APDs and electronics. The top half of the schematic represents the RF shielded APD inside the gantry while the bottom half uses optical fiber to connect to RF shielded APDs at the edge of the MR field of view. (D) Integration of RF compliant SiPM with optical fiber output obviates the need for RF shielding of PET components.

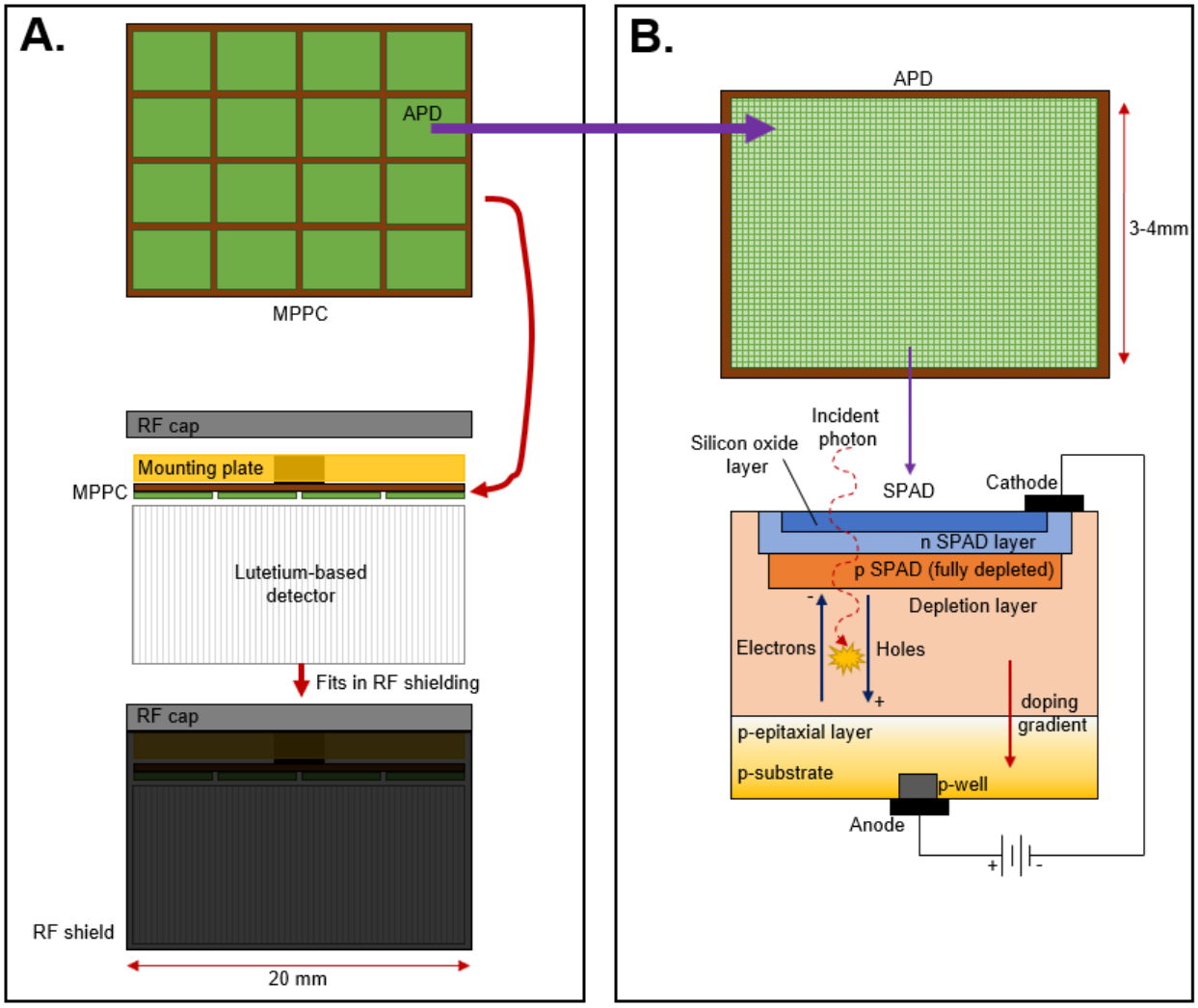

Figure 6: (A) The MPPC array is comprised of multiple APDs and mounted to the lutetium-based detector which is housed in a light proof RF shield. These small individual MPPC units (2cm) make up the PET detector system. (B) The APD (in this case a G-APD) is comprised of pixels (SPAD). The layers of the SPAD use a silicon dioxide layer through which incident photons interact in a depletion layer. Excitation causes electron holes that migrate to positive and negative doped layers to produce a signal.

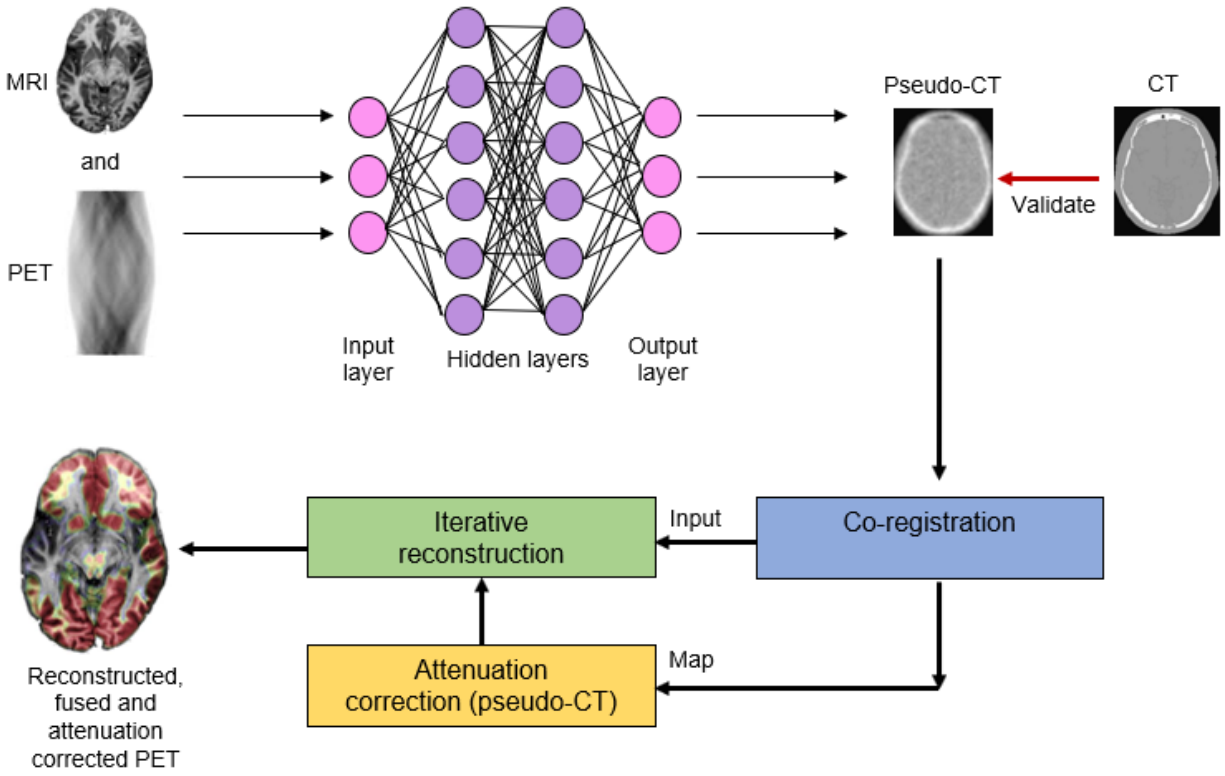

Figure 7: Model for potentially using CNN for improved pseudo-CT attenuation correction in PET/MRI. Adapted from *16* with permission.